Journal of the Physical Society of Japan
Vol. 67, No. 12, December, 1998, pp. 4084-4088

Effects of Relativistic Binary Collisions on PIC Simulation of Laser Plasmas

Yasuhiko SENTOKU, Kunioki MIMA, Yasuaki KISHIMOTO[1] and Mitsuru HONDA[2]

Institute of Laser Engineering, Osaka University, Suita 565-0871
[1] *Japan Atomic Energy Research Institute, Naka-gun 311-0100*
[2] *Max Planck Institute for Quantum Optics, Garching, Germany*

(Received May 6, 1998)

Relativistic binary collision effects on the intense laser plasma interactions are investigated by introducing the Monte Carlo Coulomb model into a particle simulation code. Our collision model is fully relativistic, where the collision frequency is calculated in the frame work of relativistic electro-dynamics. By the particle simulation, the following two phenomena which are important in laser plasmas are investigated. The first one is for the electron heat transport in a steep temperature gradient and the second is for the electron energy distribution function of plasmas heated by a relativistic intensity laser irradiation. The results of the simulations are compared with the results of numerical analysis of the Fokker-Planck equation.

KEYWORDS: PIC simulation, binary collision, Fokker-Plank, laser plasmas

§1. Introduction

Recently, compact terawatt lasers have been developed, and the intensity of sub-picosecond lasers is over $10^{18}\,\mathrm{W/cm^2}$.[1)] In dense plasmas produced by intense short pulse lasers, the plasmas are relativistic, and the highly nonequilibrium. In order to investigate physical processes in such laser plasmas, for examples, energy transport, generation of hard X-ray and inverse Faraday effects, it is important to know the electron velocity distribution functions in plasmas which depend on the collisional laser heating processes. Many previous works have investigated the electron velocity distribution by solving the Fokker-Planck equation. However, in order to simulate the laser plasma interactions which include both the nonlinear effects and the collisional processes, it is necessary to develop a relativistic binary collision model for the electro magnetic particle in cell (EM-PIC) code. Historically, first binary collision model was developed by Oliphant and Nielson to simulate the shock wave in neutral gases.[2)] In their model, the scattering angles are given on the basis of the local collision frequency. Takizuka and Abe utilized this model for the plasma simulations.[3)] In their model, the Debye scale computational meshes are used, and in each mesh, particles are scattered by the binary collision process which conserves energy and momentum perfectly. The collision frequency depends on the relative velocity of the pairing particles, and collisions of the same species and the interspecies could be considered. Recently, using EM-PIC code with this binary collision model, Lawson *et al.* simulated interactions of ultrashort intense laser pulses with solid-density targets.[4)] We extended the binary collision model developed by Takizuka and Abe to the relativistic case.

In our model, the exchanges of energy and momentum between two particles are fully relativistic and the collision frequency is calculated by the Born approximation. Generally, the particle simulations including the binary collision model need very long Computer time, because both the short time scale interactions of laser-plasma and the long time scale as collisional processes have to be calculated.

In order to accelerate the calculation, the collisional routines are not executed in every simulation time step. Also, by integrating the vector operation ratio, our one dimensional practical simulation takes $1.2 \simeq 2$ times longer computation time than that without collision routine. In this paper, we explain the relativistic binary collision model in §2. In §3, in order to check the validity of our code, we simulate the thermal conduction in a steep temperature gradient. In §4, the electron energy distribution functions are investigated for plasmas which are heated by relativistic intensity laser irradiation. The result is compared with that of the Fokker-Planck simulation. Section 5 is devoted to Conclusion.

§2. Relativistic Binary Collision Model

We introduce here the relativistic binary collision model for the small angle scattering. The pairs of particles suffering binary collisions are determined at random in a spatial cell. This cell, namely a grid of the simulation, is defined by the Debye length of the initial plasma temperature. These pairing procedures are the same as those in the Takizuka and Abe model.[3)] After the pairing process, the energy and the momentum exchanges are calculated on each pairs. These calculations are done in the center of mass (COM) frame of the two particles, and transferred back to the laboratory frame.

2.1 Center of mass frame

When two particles, of which masses are m_1 and m_2, have velocities of $\mathbf{v}_1$ and $\mathbf{v}_2$ in the laboratory frame, their COM frame moves with respect to the laboratory frame

with the velocity;

$$\mathbf{v}_{cm} = \frac{\gamma_1 m_1 \mathbf{v}_1 + \gamma_2 m_2 \mathbf{v}_2}{\gamma_1 m_1 + \gamma_2 m_2}. \tag{2.1}$$

In the COM frame, the particle velocities are calculated by the Lorentz transform to obtain.

$$\mathbf{v}_{i,cm} = \frac{(\gamma_{cm}-1)\frac{\mathbf{v}_{cm}\cdot\mathbf{v}_i}{\mathbf{v}_{cm}^2}\mathbf{v}_{cm} + \mathbf{v}_i - \gamma_{cm}\mathbf{v}_{cm}}{\gamma_{cm}\left(1-\frac{\mathbf{v}_{cm}\cdot\mathbf{v}_i}{c^2}\right)}, \quad i=1,2 \tag{2.2}$$

where $\gamma_{cm} = (1 - v_{cm}^2/c^2)^{-1/2}$ and c is the speed of light. In the COM frame, the sum of the momentum of two particles is zero.

$$\mathbf{P}_1 + \mathbf{P}_2 = 0. \tag{2.3}$$

Through the collision process, the total momentum is conserved. Equation (2.3) and the energy conservation mean that before and after the collision, the magnitude of momentum of each particle is invariant,

$$|\mathbf{P}_1| = |\mathbf{P}_2| = |\mathbf{P}_1'| = |\mathbf{P}_2'| = p, \tag{2.4}$$

where, p is the momentum amplitude. This enables us to calculate the scattering process in term of the method of Rutherford scattering.

2.2 *Rotating the frame*

As for describing the scattering process in the code, we rotate the coordinate system of the momentum space to the system in which P_z-axis is aligned along the momentum vector $\mathbf{P}_1$. This transformation is represented by the following equation;

$$\begin{pmatrix} \cos\theta\cos\phi & \cos\theta\sin\phi & -\sin\theta \\ -\sin\phi & \cos\phi & 0 \\ \sin\theta\cos\phi & \sin\theta\sin\phi & \cos\theta \end{pmatrix} \begin{pmatrix} p_x \\ p_y \\ p_z \end{pmatrix} = \begin{pmatrix} 0 \\ 0 \\ p \end{pmatrix}. \tag{2.5}$$

Here, θ is the angle between P_z-axis and the vector $\mathbf{P}_1$ and ϕ is the angle between P_x-P_z plane, where P_x, P_y and P_z-axis are for th COM frame. Next, we calculate the collision frequency by choosing a scattering angle Θ randomly.

2.3 *Collision frequencies*

The relativistic collisional frequency is given by the following form.[5)]

$$\nu_{12} = \frac{4\pi(e_1 e_2)^2 n_l L}{p_{rel}^2 v_{rel}}, \tag{2.6}$$

where p_{rel} and v_{rel} are the relative momentum and velocity between two particles respectively, e_1 and e_2 are the charge of each particle, n_l is the lower density among n_1 and n_2, and L is the Coulomb logarithm. In the relativistic energy range, the condition $|e_1 e_2|/\hbar v_{rel} > 1$ is not satisfied, so the ratio of the minimum scattering angle θ_{min} to the maximum θ_{max} is given by

$$\theta_{min}/\theta_{max} = \frac{\hbar}{\lambda_D m_{12} v_{rel}}, \tag{2.7}$$

where m_{12} is the reduced mass, $\hbar$ is the Planck constant and λ_D is the Debye length. Then the Coulomb logarithm is given by

$$L = \log\left(\frac{\lambda_D m_{12} v_{rel}}{\hbar}\right). \tag{2.8}$$

The scattering angle Θ is chosen randomly from the distribution of Θ that has the zero mean value, and the variance is given by

$$\langle \tan^2(\Theta/2)\rangle = \nu_{12} N_c \gamma_{cm} \Delta t, \tag{2.9}$$

where Δt is the simulation time step and N_c is the number of time steps between subsequent sampling times for calculation of the collision. We set $N_c \Delta t \simeq \tau_c/50$, where τ_c is the relaxation time, namely, the mean free time.

2.4 *Scattering process*

Through the binary collision process, the magnitude of the momentum p is unchanged, but only the direction is changed.

$$(0,0,p) \to (p\sin\Theta\cos\Phi,\ p\sin\Theta\sin\Phi,\ p\cos\Theta), \tag{2.10}$$

where the azimuthal angle Φ distributes from 0 to 2π uniformly. Then the momentum change of the particle in the collision is given in the COM frame as follows,

$$\Delta p_x = (p_x/p_\perp)p_z \sin\Theta\cos\Phi - (p_y/p_\perp)p\sin\Theta\sin\Phi - p_x(1-\cos\Theta), \tag{2.11}$$

$$\Delta p_y = (p_y/p_\perp)p_z \sin\Theta\cos\Phi + (p_x/p_\perp)p\sin\Theta\sin\Phi - p_y(1-\cos\Theta), \tag{2.12}$$

$$\Delta p_z = -p_\perp \sin\Theta\cos\Phi - p_z(1-\cos\Theta), \tag{2.13}$$

where, $p_\perp = (p_x^2 + p_y^2)^{1/2}$. By using $\Delta\mathbf{P} = (\Delta p_x, \Delta p_y, \Delta p_z)$, we get the momentum after the collision,

$$\mathbf{P}_1' = \mathbf{P}_1 + \Delta\mathbf{P}, \tag{2.14}$$

$$\mathbf{P}_2' = \mathbf{P}_2 - \Delta\mathbf{P}. \tag{2.15}$$

Finally, the velocities in the laboratory frame is obtained by

$$\mathbf{v}_i' = \frac{(\gamma_{cm}-1)\frac{\mathbf{v}_{cm}\cdot\mathbf{v}_{i,cm}'}{\mathbf{v}_{cm}^2}\mathbf{v}_{cm} + \mathbf{v}_{i,cm}' + \gamma_{cm}\mathbf{v}_{cm}}{\gamma_{cm}\left(1+\frac{\mathbf{v}_{cm}\cdot\mathbf{v}_{i,cm}'}{c^2}\right)}, \quad i=1,2. \tag{2.16}$$

These calculations are done for all binary pairs.

§3. Simulations of Heat Conduction in a Steep Temperature Gradient

In the steep temperature gradient which scale length is equal to or shorter than the electron mean free path, as in the plasmas produced by high power lasers, the Spitzer-Harm (S-H) thermal conductivity is no more valid. According to the Fokker-Planck simulation by Bell *et al.*[6)] and the related theory by Y. Kishimoto *et al.*, the heat flux is an order of magnitude less than that of the S-H theory,[8)] and not proportional to the local temperature gradient. Using the parameter of the Bell's simulation, we investigated the energy transport in the steep

temperature gradient plasma by our new collisional PIC code. In this code, the plasma is treated as 1D3V (one spatial, three velocity dimension) and is coupled with the electro magnetic equations. The simulation setting are following; the plasma has the uniform density and the uniform temperature initially, and distributes in 0 to 2048 λ_D area. Ions are mobile to take into account the electron-ion binary collision model, and its charge state Z and mass M_i are 4 and 10000, respectively. The initial velocity distributions of ion and electron are set to be Maxwellian. In this simulation, time and space are normalized by plasma frequency ω_p and the Debye length λ_D, respectively. The initial thermal velocity, which is given by $\omega_p\lambda_D$, is equal to 1.0 in this unit. The plasma parameter Λ, defined by $n\lambda_D^3$, is set to be 100. The temperature T and the heat flux Q are defined by $\frac{1}{2}m_e\langle v^2\rangle$ and $\frac{1}{2}m_e\langle v^2 v_x\rangle$, respectively. When the initial temperature is 1 keV, these parameters correspond to the plasma density of $10^{22}\,\mathrm{cm}^{-3}$. 81920 particles and 2048 meshes are used in this simulation.

Starting the simulation, the plasma is quickly heated up to 4 times the initial temperature in the region $0 < x < 350$. The electrons are numerically heated up in order to keep the temperature to be the 4 times initial temperature, according to the following equation.

$$\frac{\mathrm{d}v^2}{\mathrm{d}t} = \alpha\frac{T_h - T}{T_h}, \tag{3.1}$$

where v is the electron velocity, T_h is the required high temperature, α is the adjustable parameter. Equation (3.1) would keep the initial distribution, if the electrons couldn't escape from the hot region. α is set to the value which is equal to the Bell's simulation, then the plasma temperature becomes 4 times of the initial temperature after about 100 time. After that, the heating continues to keep the temperature constant.

Figure 1 shows the normalized temperature $\langle v^2\rangle$ and heat flux $\langle v^2 v_x\rangle$ profiles at 1000 and 2000 time steps, which are very similar to the Bell's results, the heat flux is maximum at the edge of the heated region. The maximum heat flux is evaluated to be $Q \simeq 0.1nkT(kT/m)^{1/2}$. Here, we note that the electron drift velocity $\langle v\rangle$ is negligible as it is also shown by Bell *et al.* Figure 2 shows the heat flux Q versus the temperature scale length $L = T(\mathrm{d}T/\mathrm{d}x)^{-1}$. The temperature scale length is normalized by the electron mean free path $\lambda_e = \sqrt{\langle v^2\rangle}/\nu_e$, here ν_e is electron-ion collision frequency of the thermal velocity and is given by eq. (2.6), and the heat flux is normalized by the local free-streaming limit $Q_f = nkT(kT/m)^{1/2}$. λ_e and Q_f are evaluated at every grid and every time, because the velocity distribution is time dependent non-Maxwellian due to the hot electrons, which are generated in the heat region and penetrate into the low temperature region. The solid line shows the S-H heat flux in Fig. 2. This figure shows that the heat flux is the divalent function of the temperature gradient. We can see in the heated region the heat flux is one order of magnitude less than the S-H theory and in the low temperature region, because of hot electrons penetrated from the heat region, the heat flux exceeds the S-H value. These results are also well agreed with Bell's

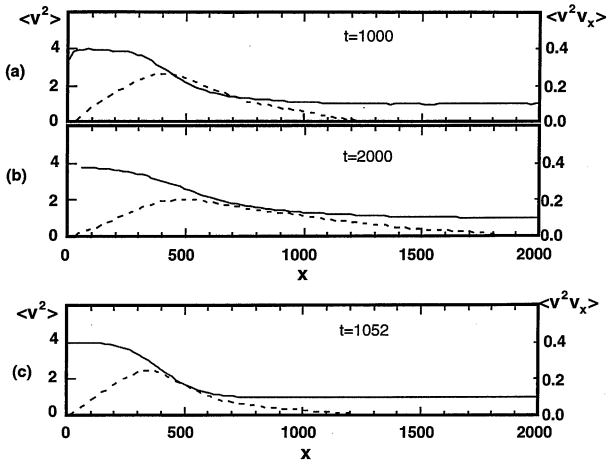

Fig. 1. Plots of the temperature $\langle v^2\rangle$ (solid line) and heat flux $\langle v^2 v_x\rangle$ (dotted line) profiles. These results are averaged over the plasma oscillating period. (a) and (b) are simulation results at times $t = 1000$, $t = 2000$ respectively, and (c) shows Bell's result[6] at $t = 1052$.

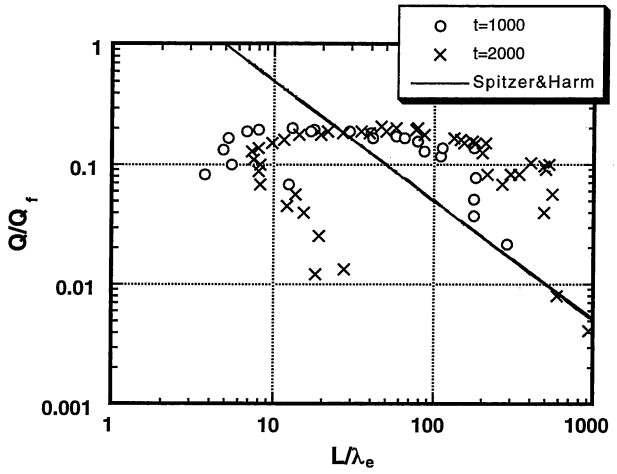

Fig. 2. Plot of the heat flux Q against the temperature scale length L. The heat flux is normalized by $Q_f = nT(kT/m)^{1/2}$ and the temperature scale length is normalized by the mean free path of electron λ_e. The solid line shows the Spitzer-Harm heat flux.

ones. From these figures, it is verified that the present collisional particle simulation code well reproduces the Bell's Fokker-Planck results.

§4. Electron Energy Distributions of Plasmas Heated by Ultra-Intense Lasers

Langdon derived the Fokker-Planck equation in the oscillating electric field and reported that when $Zv_o^2/v_e^2 \geq 1$ for the laser quiver velocity v_o, the velocity distribution of plasma electron becomes non-Maxwellian, where v_e is the electron thermal velocity.[9] We extend the Langdon's Fokker-Planck equation to the relativistic regime. The first two kinetic equations, using the Legendre spherical expansion and averaged over the solid angle, are

$$\frac{\partial f_0}{\partial t} + \frac{v}{3}\nabla\cdot\mathbf{f}_1 - e(\mathbf{E}_{em}+\mathbf{E}_2)\cdot\frac{1}{3p^2}\frac{\partial}{\partial p}(p^2\mathbf{f}_1) = 0, \tag{4.1}$$

$$\frac{\partial \mathbf{f}_1}{\partial t} - e(\mathbf{E}_{em}+\mathbf{E}_2)\frac{\partial f_0}{\partial p} = -\nu_{ei}\mathbf{f}_1, \tag{4.2}$$

where, v and p are the absolute value of velocity and momentum, $\mathbf{E}_{em}$ is the electro magnetic (E-M) wave given by $E\sin(\omega t - kz)\hat{\mathbf{x}}$ and $\mathbf{E}_2$ is the longitudinal electric field which is induced by the $\mathbf{v}\times\mathbf{B}$ longitudinal electron oscillation, namely the second harmonic oscillation associated with the ponderamotive force. $\mathbf{E}_2$ is approximately evaluated, as follows,

$$\mathbf{E}_2 = \frac{1}{e\epsilon}\frac{\omega_p^2}{4\omega^2}\frac{k}{m_e}p_o^2\sin 2(\omega t - kz)\hat{\mathbf{z}}, \qquad (4.3)$$

here, $\epsilon = 1-\omega_p^2/4\omega^2$ is the plasma dielectric function, m_e is the mass of electron and $p_o = eE/\omega$ is the oscillating momentum. Calculating $\mathbf{f}_1$ from eq. (4.2) and inserting it into eq. (4.1), we get the time averaged Fokker-Planck equation in the E-M wave field,

$$\frac{\partial f_0}{\partial t} - \frac{1}{3p^2}\frac{\partial}{\partial p}\left[\frac{p^2}{2}\frac{p_o^2\omega^2\nu_{ei}}{\omega^2+\nu_{ei}^2}\frac{\partial f_0}{\partial p}\right] - \frac{1}{3p^2}\frac{\partial}{\partial p}\left[\frac{p^2}{2}\frac{p_{o2}^2(2\omega)^2\nu_{ei}}{4\omega^2+\nu_{ei}^2}\frac{\partial f_0}{\partial p}\right] = 0, \qquad (4.4)$$

where $p_{o2} = eE_2/(2\omega)$ is the oscillating momentum and $\nu_{ei} = 4\pi n_e Z e^4\gamma m_e \ln\Lambda/p^3$ is the electron-ion collision frequency. Note that the eq. (4.4) is valid only when the electron temperature is sufficiently lower than 500 keV. The second term on left hand side of eq. (4.4) is the relativistic Langdon's operator. We simulated the light absorption by inverse bremsstrahlung and the results are compared with the numerical evaluation of eq. (4.4). The initial electron momentum distribution is assumed Maxwellian with the electron temperature of 1 keV. We also use the following simulation parameters: ion charge state $Z = 16$, ion density $10^{21}\,\mathrm{cm}^{-3}$, the plasma frequency $\omega_p = 7.1\cdot 10^{15}\,\mathrm{rad/sec}$, the laser frequency $\omega = 1.4\omega_p$ corresponded to the laser wave length 188 nm, the laser intensities $8\cdot 10^{17}, 3\cdot 10^{18}$ and $1.2\cdot 10^{19}\,\mathrm{W/cm}^2$. At these intensities the dimensionless light amplitude $\alpha = p_o/m_e c = 0.05$, 0.1 and 0.2. The duration of heating time was 14 fsec, number of simulation particles was 34816 and number of meshes was 256. Here, we considered only the electron and ion scattering as it is assumed in the eq. (4.4). Figures 3(a)–3(c) show the electron momentums distribution after heating. In the simulation, the momentum distribution is calculated from the electron's motion which is averaged over the laser oscillating period. The solid lines are obtained by the numerical analysis of eq. (4.4) and the dot points express the simulation's results in Figs. 3. Although the distribution in the low energy region does not agree with the analytic results of eq. (4.4), because of finite number of simulation particle, the overall results of the simulations are in good agreement with those of the relativistic Fokker-Planck analysis.

Figure 4 shows that the comparison of the electron momentum distributions between PIC simulation and Fokker-Planck analysis when $\omega = 2.0\omega_p$, other parameters are same as those of Figs. 3. In this case, the result does not agree each other. The maximum growth rate of the stimulated Raman scattering is given[10]

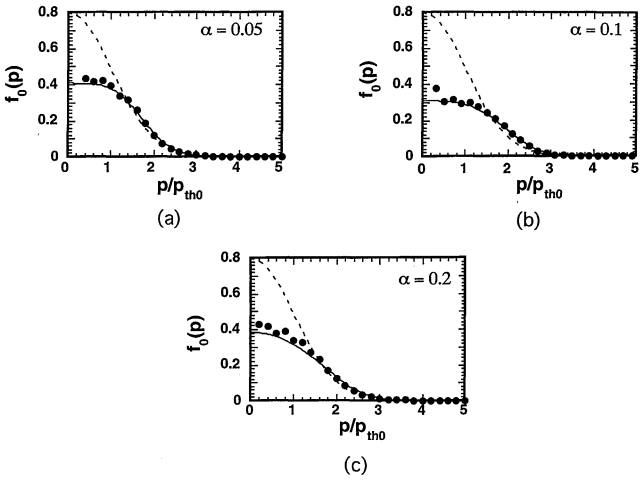

Fig. 3. Plots of the electron momentum distributions after heating at 14 fsec. At $t = 0$, the electron momentum distribution was assumed the Maxwellian (dotted line). The solid line shows the results of eq. (4.4) and the point plots show the simulation results. (a) is for $\alpha = p_o/m_e c = 0.05$, (b) is for $\alpha = 0.1$ and (c) is for $\alpha = 0.2$.

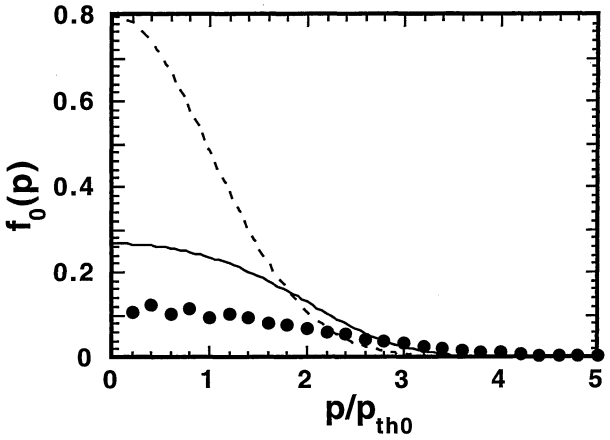

Fig. 4. Plot of the electron momentum distribution for the case of $\omega = 2\omega_p$. The electron initial distribution is the Maxwellian (dotted line). Here α is 0.2 and the other parameters are same as that of Figs. 3. The solid line shows the results of eq. (4.4) and the point plots show the simulation results.

$$\gamma_R \simeq \frac{\omega_p^2}{2\sqrt{2}\omega}\frac{v_o}{c}, \qquad (4.5)$$

where v_o is the oscillating velocity. The growth rate is evaluated $\gamma_R \sim 2.51\cdot 10^{14}$, in the case of $\alpha = 0.2$ and $\omega = 2.0\omega_p$. So the stimulated Raman scattering is possible to grow sufficiently even in ten fsec. In Fig. 4, the simulation result doesn't fit to the line of the Fokker-Planck analysis, because the some electrons are accelerated by plasma waves which are excited by the stimulated Raman scattering. This is explained by the phase plot of the electron's longitudinal motion in Fig. 5. These nonlinear effects are not included in eq. (4.4).

Figure 6 shows the analytical results of electron momentum distributions for the relativistic case and non relativistic case at 14 fsec. In these analysis, all parameters are same as that of Figs. 3. The solid lines show the results of eq. (4.4) and the dotted lines show the results

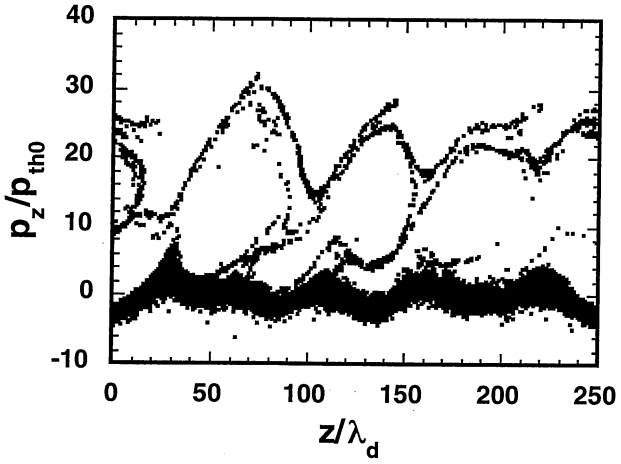

Fig. 5. The phase plot of the electron longitudinal momentum for $\alpha = 0.2$ and $\omega = 2\omega_p$ at 14 fsec.

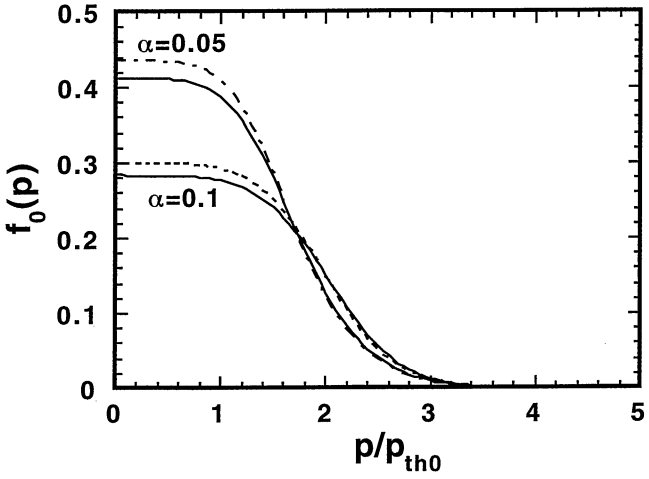

Fig. 6. Plots of the electron momentum distributions for the relativistic case and non relativistic case. All parameters are same as that of Fig. 3. The solid lines show the results of eq. (4.4) and the dots lines show the results of non relativistic case same as the Langdon's Fokker-Plank equation.[9]

of non relativistic case same as the Langdon's Fokker-Planck equation.[9] The results are slightly different between relativistic and non relativistic case for these parameters. However the difference of two equations will be significant near the cut off region where $\omega_p \sim \omega$ and/or in the higher intensity region; $p_o/mc \geq 1$, since the ratio of $p_{o2}/p_o \sim (\omega_p/2\omega)^2 \cdot (p_o/m_e c)$.

§5. Conclusion

We investigated the two phenomena which are important in laser plasmas using one dimensional PIC code with the relativistic binary collision. The first one is for the electron heat transport in a steep temperature gradient. We demonstrated the non local heat transport by PIC code and checked the validity by comparing to the Fokker-Planck simulation. The second one is for the electron energy distribution function of plasmas heated by a relativistic intensity laser irradiation. We derived the relativistic Fokker-Planck equation in the electro magnetic wave field and evaluated numerically to compare with the results of PIC simulation. We got the almost same results from the both approaches. The relativistic binary collision model is able to simulate the heat transport and the laser absorption for the intense laser plasma correctly and effectively, it is equivalent to the Fokker-Planck analysis as we have shown in this paper.

Acknowledgements

Two of the authors, Y.S and Y.K, would like to thank Mr. H. Watanabe of the Research Organization for Information Science and Technology at Japan Atomic Energy Research Institute for his computational support.

1) G. Mourou and D. Umstadter: Phys. Fluids B **4** (1992) 2315.
2) T. A. Oliphant and C. W. Nielson: Phys. Fluids **13** (1970) 2103.
3) T. Takizuka and H. Abe: J. Comput. Phys. **25** (1977) 205.
4) W. S. Lawson, P. W. Rambo and D. J. Larson: Phys. Plasmas **4** (1997) 788.
5) E. M. Lifshitz and L. P. Pitaevskii: *Physical Kinetics* (Pergamon Press, Oxford, 1981) Chap. 4.
6) A. R. Bell, R. G. Evans and D. J. Nicholas: Phy. Rev. Lett. **46** (1981) 243.
7) Y. Kishimoto, K. Mima and M. G. Haines: J. Phys. Soc. Jpn. **57** (1988) 1972.
8) L. Spitzer and R. Harm: Phys. Rev. **89** (1953) 977.
9) A. B. Langdon: Phy. Rev. Lett. **44** (1980) 575.
10) W. L. Kruer: *The Physics of Laser plasma Interactions* (Addision-Wesley, NewYork, 1988) p. 79.